# Longitudinal distribution of fast charged particles traversing through matter

Takao Nakatsuka
*Okayama Shoka University, Okayama, Japan*
(Received 19 June 1997; published 31 July 1998)

The Yang equation describing the excess-path-length distribution under the multiple Coulomb scattering process is improved to take into account the continuous energy loss by ionization. The equation gives the simultaneous distribution of the direction of motion, lateral displacement, and longitudinal distribution of fast charged particles traversing through matter. The equation is analytically solved completely in the image space of Laplace transforms and the excess-path-length distributions corresponding to the most general conditions of geometry are obtained by the inverse Laplace transforms, exactly in series expansion or asymptotically through the saddle point method. The distributions after receiving ionization loss are indicated in figures and the effect of including ionization loss is discussed. The means and the variances of the distribution are also tabulated. [S0556-2821(98)02613-7]

PACS number(s): 11.80.La, 02.50.Ey, 29.40.Rg, 96.40.Pq

## I. INTRODUCTION

Since Fermi wrote down the multiple Coulomb scattering theory in the Fokker-Planck approximation [1] it has become very simple and plain to investigate fluctuation properties concerning the passage of charged particles traversing through material. It gave a Gaussian distribution of Williams type [2] for both the probability densities of the deflection angle and the lateral displacement, respectively, and the normal distribution for the simultaneous distribution of both elements, so that the method has been called the Gaussian approximation ever since [3]. All the distributions are obtained as exact analytical solutions through a fairly fundamental way of mathematics. Efforts to extend the applicability of the Fermi equation have been continued. The equation taking into account energy loss by ionization was solved by Eyges [4] by applying a simple alteration of the variable. The improvement of the Fermi equation to simultaneously take into account the excesses of the path length was proposed by Yang [5] and was solved in the most general condition in our preceding paper (PP) [6].

Although the Gaussian approximation is less accurate in describing the multiple scattering process than the Molière method [7,8], the fact that we can get the simultaneous distribution [3,9] for the arbitrary combination among those elements is the most valuable feature of the Gaussian approximation. From the practical point of view, it was a defect of the Molière theory that not much distributions other than the single distributions for any linear combination of the deflection angle and the lateral displacement had been obtained from the theory itself [3,10]. It should be noticed that Kamata and Nishimura proposed a method to build the Molière theory in the Fermi formulation [11,12], equivalent in mathematics [6]. According to the Kamata-Nishimura formulation, the probability density under the Molière theory can be obtained as a power series in $1/\Omega$ in the space of Fourier transforms, where the first term is the solution of a diffusion equation under the Fermi formulation and the following terms are obtained successively by solving the same equation with the known inhomogeneous term containing the precedingly determined term, as Kamata and Nishimura applied in their cascade shower theory [11,12] and we did in the excess-path-length distribution in PP. Thus we can say that the multiple scattering theory under the Fermi formulation is not a different theory from the Molière theory but rather they are equivalent in the way in which the latter can be constructed from the former.

The very significance of the Yang equation is that it has enabled us to simultaneously describe the longitudinal distribution of fast charged particles traversing through matter, just as the Fermi equation simultaneously described the lateral distribution. The excess-path-length distribution of Yang gives the detour distribution of arrived particles observed at a fixed thickness. From the other point of view, the Yang equation gives the deficiency distribution of contracted thickness of traverse from the actual path length as formulated by Scott [13]. The Yang and the Scott equations are mathematically equivalent to each other under the small angle and the Fokker-Planck approximations.

According to the latter point of view, the existing analytical results describing the properties of charged particles propagating in matter, e.g., the angular distribution [7,8], the lateral distribution [1], the energy-loss distribution by collision [14–17], and the range and its fluctuation of charged particles [15,18–20], must be corrected in the longitudinal direction of development since the visually observed path length is reduced from the actual one measured along the trajectory itself as noted by Rossi [18] and others [21–23]. Modern computer codes of Monte Carlo simulation [24–26] are not relevant to this correction in principle as they trace particle passages as actual propagations. But some problems remain also in this method. The highly-accurate multiple scattering theories used in the code describe only the angular distribution, so that the lateral displacement and the excess of path length are approximated in the code, together with their correlations. And the step size applied in the code cannot be taken infinitesimal, so that too long a step size might cause the difference between the step size and the actual path length. To determine the appropriate step size or to examine the reliability of correlation among those passage elements

 

[9], investigations using Fermi and Yang theory is inevitable [27,28].

In PP, we showed the general solution of the Yang equation and gave the simultaneous distribution among the direction of motion, the lateral displacement, and the excess of path length for charged particles in the most general conditions of geometry, assuming the energy of charged particles constant. In actual propagations, charged particles lose their energy by ionizations and radiations [1], so that particles with the decreasing energy receive more effects from the multiple scattering process. For the particles of moderately relativistic energy [9] and even those of higher energy before occasional radiations of high-energy photons, the ionization loss plays dominant roles for the energy dissipation of the particles. So we will improve the Yang equation by taking into account continuous energy loss by the ionization and get the distributions in the same geometrical conditions as PP. This improvement will make the existing analytical results describing the propagation of charged particles more reliable by correcting the predictions in the longitudinal direction and making the excess distribution of path length more applicable in tracing charged particles in simulations [29] or designing and analyzing experiments concerning charged particles [9].

## II. THE YANG EQUATION WITH IONIZATION

Charged particles traversing through materials undergo the multiple Coulomb scattering, so that they change their directions of motion $\vec{\theta}$ and lateral displacements $\vec{r}$, as well as excesses of path length $\Delta$. Starting from the Yang equation, we obtained in PP the correlated probability densities among these components of charged particles, having passed $t_0$ with $\vec{\theta}_0$, $\vec{r}_0$, and $\Delta_0$ and having reached $t$ with $\vec{\theta}$, $\vec{r}$, and $\Delta$: $F(t,\theta_y,y,\Delta_y,t_0,\theta_{y0},y_0,\Delta_{y0})d\theta_y dy d\Delta_y$ for projected components to the $t$-$y$ plane, and $A(t,\vec{\theta},\vec{r},\Delta,t_0,\vec{\theta}_0,\vec{r}_0,\Delta_0)d\vec{\theta}d\vec{r}d\Delta$ for spatial components. This time we will get probability densities of the same conditions taking into account energy loss by ionization.

We improve the Yang equation as follows:

$$\frac{\partial F}{\partial t}+\theta\frac{\partial F}{\partial y}-\frac{1}{w^2}\frac{\partial^2 F}{\partial\theta^2}+\frac{1}{2}\theta^2\frac{\partial F}{\partial\Delta}-\varepsilon\frac{\partial F}{\partial E}$$
$$=\delta(t-t_0)\,\delta(E-E_0)\,\delta(\theta-\theta_0)\,\delta(y-y_0)\,\delta(\Delta-\Delta_0), \tag{1}$$

where $t$, $\vec{r}$, and $\Delta$ are all measured in radiation lengths [1]. The last term on the left-hand side is added to include the effect that the charged particles with the initial energy $E_0$ dissipate their energy in constant rate, $\varepsilon$ in unit radiation length [1,12], in the small angle approximation [3]. In the third term, we approximate $w$ by

$$w=2E/E_s, \tag{2}$$

instead of $w=2pv/E_s$ of PP, as traditional works of, e.g., Landau [30], Nishimura [12], and others [31], which is a good approximation when the rest energy is small enough compared to $E$. We can also put zeros to $t_0$, $y_0$, and $\Delta_0$, due to the translational invariance of those variables without loss of generality, as PP.

Under our assumption of ionization, the energies of charged particles are determined by traversed thickness as

$$E=E_0-\varepsilon t, \tag{3}$$

so that, if we take into account this dependence of $E$ on $t$, the last term on the left-hand side of Eq. (1) vanishes. The maximum thickness $R$ the particles traverse in this process is called the range in the ionization process [1,18]. We introduce a tentative constant $k$ in place of $1/R$:

$$R=E_0/\varepsilon \quad \text{and} \quad k=1/R. \tag{4}$$

Then $kt$ means the fraction of traversed thickness to $R$ which is identical with the fraction of dissipated energy to $E_0$, and gives the supplementary relation with the fractional energy $E/E_0$:

$$kt=t/R=1-E/E_0. \tag{5}$$

Applying the Fourier and Laplace transforms with $y$ and $\Delta$, respectively, we get

$$F=\frac{1}{4\pi^2 i}\int d\lambda e^{\Delta\lambda}\int e^{iy\eta}\psi(t,\theta,\eta,\lambda,\theta_0)d\eta. \tag{6}$$

Then, the diffusion equation (1) becomes

$$\frac{\partial\psi}{\partial t}+i\eta\theta\psi-\frac{1}{w_0^2(1-kt)^2}\frac{\partial^2\psi}{\partial\theta^2}+\tfrac{1}{2}\lambda\theta^2\psi=\delta(t)\,\delta(\theta-\theta_0), \tag{7}$$

where $w_0$ is $w$ of the incident particle. Introducing new variables

$$\omega'^2=\frac{\lambda}{2w_0^2}+\frac{k^2}{16},\quad q=w_0\sqrt{\omega'}\sqrt{1-kt}\left(\theta+\frac{i\eta}{\lambda}\right), \tag{8}$$

the homogeneous equation of (7) becomes

$$\frac{1-kt}{\omega'}\left(\frac{\partial}{\partial t}+\frac{\eta^2}{2\lambda}\right)\psi=\left(\frac{\partial^2}{\partial q^2}+\frac{k}{2\omega'}q\frac{\partial}{\partial q}-\frac{\lambda}{2w_0^2\omega'^2}q^2\right)\psi; \tag{9}$$

thus it can be solved by separating variables:

$$\psi=f(t)g(q)e^{-(1/8)kq^2/\omega'}. \tag{10}$$

The solution satisfying inhomogeneous term of Eq. (7) is obtained by the linear combination of orthogonal functions:

$$\psi = w_0\sqrt{\omega'}(1-kt)^{k^{-1}\omega'+1/4}\exp[-\tfrac{1}{2}\eta^2 t/\lambda - \tfrac{1}{8}w_0^2 k(1-kt)(\theta+i\eta/\lambda)^2 + \tfrac{1}{8}w_0^2 k(\theta_0+i\eta/\lambda)^2]$$
$$\times\sum_{n=0}^{\infty}(1-kt)^{2nk^{-1}\omega'}\psi_n(w_0\sqrt{\omega'}(\theta_0+i\eta/\lambda))\psi_n(w_0\sqrt{\omega'}\sqrt{1-kt}(\theta+i\eta/\lambda)), \tag{11}$$

where $\psi_n(x)$ is the same function as defined in PP:

$$\psi_n(x) = (\sqrt{\pi}2^n n!)^{-1/2}H_n(x)e^{-x^2/2}. \tag{12}$$

Sum of the series (11) can be derived by using the generalized generating function indicated in Eq. (2.9) of PP. Introducing the new variables [32]

$$t' = -k^{-1}\ln(1-kt), \quad \text{or} \quad \tau = \tfrac{1}{2}kt' = \tfrac{1}{2}\ln(E_0/E), \tag{13}$$

and

$$\sqrt{s'} = 2t'\omega', \tag{14}$$

we get

$$\psi = \frac{w_0\sqrt{k}e^{-\tau/2}}{[8\pi\tau\sinh\sqrt{s'}/\sqrt{s'}]^{1/2}}\exp\left(-\frac{w_0^2 k e^{-\tau}}{8\tau\sinh\sqrt{s'}/\sqrt{s'}}\left\{\frac{\eta^2}{\lambda^2}[2-2\cosh\tau\cosh\sqrt{s'}+(\tau^{-2}s'+1)\tau\sinh\tau\sinh\sqrt{s'}/\sqrt{s'}]\right.\right.$$
$$+2\frac{i\eta}{\lambda}[(\cosh\sqrt{s'}+\tau\sinh\sqrt{s'}/\sqrt{s'}-e^{\tau})e^{-\tau}\theta+(\cosh\sqrt{s'}-\tau\sinh\sqrt{s'}/\sqrt{s'}-e^{-\tau})e^{\tau}\theta_0]$$
$$\left.\left.+[(\cosh\sqrt{s'}+\tau\sinh\sqrt{s'}/\sqrt{s'})e^{-\tau}\theta^2-2\theta\theta_0+(\cosh\sqrt{s'}-\tau\sinh\sqrt{s'}/\sqrt{s'})e^{\tau}\theta_0^2]\right\}\right). \tag{15}$$

Applying inverse Fourier transforms to $\eta$, we get

$$\xi d\theta dy = \frac{w_0^2k^2(\tau^{-2}s'-1)d\theta dy}{16\pi[2-2\cosh\tau\cosh\sqrt{s'}+(\tau^{-2}s'+1)\tau\sinh\tau\sinh\sqrt{s'}/\sqrt{s'}]^{1/2}}$$
$$\times\exp\left\{-\frac{w_0^4k^4(\tau^{-2}s'-1)^2}{256[2-2\cosh\tau\cosh\sqrt{s'}+(\tau^{-2}s'+1)\tau\sinh\tau\sinh\sqrt{s'}/\sqrt{s'}]}\right.$$
$$\times\left[\frac{32(\sinh\tau\cosh\sqrt{s'}-\tau\cosh\tau\sinh\sqrt{s'}/\sqrt{s'})e^{-2\tau}}{w_0^2k^3(\tau^{-2}s'-1)}(\theta^2-2\theta\theta_0+\theta_0^2e^{2\tau})\right.$$
$$-\frac{32(\cosh\sqrt{s'}+\tau\sinh\sqrt{s'}/\sqrt{s'}-e^{\tau})e^{-\tau}}{w_0^2k^2(\tau^{-2}s'-1)}\theta\left(y-\frac{2}{k}\theta_0e^{-\tau}\sinh\tau\right)-\frac{32(\cosh\sqrt{s'}-\tau\sinh\sqrt{s'}/\sqrt{s'}-e^{-\tau})e^{\tau}}{w_0^2k^2(\tau^{-2}s'-1)}\theta_0y$$
$$\left.\left.+\frac{8(\tau\sinh\sqrt{s'}/\sqrt{s'})e^{\tau}}{w_0^2k}y^2\right]\right\}. \tag{16}$$

Mean square spatial angle and displacement, $\langle\theta^2\rangle_{\rm av}$ and $\langle r^2\rangle_{\rm av}$, for normally-incident particles after traversing through thickness of $t$ in our process can be obtained by a method in Appendix A:

$$\langle\theta^2\rangle_{\rm av} = \frac{8}{w_0^2k}e^{\tau}\sinh\tau, \tag{17}$$

$$\langle r^2\rangle_{\rm av} = \frac{16}{w_0^2k^3}e^{-2\tau}(\cosh\tau\sinh\tau-\tau). \tag{18}$$

If we introduce nondimensional variables for deflection angle and lateral displacement,

$$\vec{\phi} = \vec{\theta}/\langle\theta^2\rangle_{\rm av}^{1/2}, \tag{19}$$

TABLE I. List of $D$'s and relating functions.

| | Functions |
|---|---|
| $D_{\mathrm{I}}$ | $(C+2\tau C')e^{-\tau}$ |
| $D_{\mathrm{II}}$ | $\frac{2\tau}{\sinh\tau}C'$ |
| $D_{\mathrm{III}}$ | $\frac{2\tau^2}{\cosh\tau\sinh\tau-\tau}\frac{C\sinh\tau-2\tau C'\cosh\tau}{s'-\tau^2}$ |
| $D_{\mathrm{gen}}$ | $\frac{4\tau^4}{(\cosh\tau\sinh\tau-\tau)e^{-\tau}\sinh\tau}\frac{1-C\cosh\tau+(s'+\tau^2)C'\sinh\pi/\tau}{(s'-\tau^2)^2}$ |
| $D_{\mathrm{X}}$ | $\frac{2\sqrt{2}\tau^2}{\sqrt{(\cosh\tau\sinh\tau-\tau)e^{-\tau}\sinh\tau}}\frac{(C+2\pi C')e^{-\tau}-1}{s'-\tau^2}$ |
| $D_{\mathrm{Y}}$ | $\frac{2\sqrt{2}\tau^2}{\sqrt{(\cosh\tau\sinh\tau-\tau)e^{-\tau}\sinh\tau}}\frac{(C-2\pi C')e^{\tau}-1}{s'-\tau^2}$ |
| $C$ | $\cosh\sqrt{s'}$ |
| $C'$ | $\frac{1}{2}\sinh\sqrt{s'}/\sqrt{s'}$ |

$$\vec{\rho}=\vec{r}/\langle r^2\rangle_{\mathrm{av}}^{1/2}\ , \tag{20}$$

together with those relative to the axis of the incident track,

$$\vec{\phi}'=(\vec{\theta}-\vec{\theta}_0)/\langle\theta^2\rangle_{\mathrm{av}}^{1/2}=\vec{\phi}-\vec{\phi}_0, \tag{21}$$

$$\vec{\rho}'=(\vec{r}-\vec{\theta}_0 t)/\langle r^2\rangle_{\mathrm{av}}^{1/2}=\vec{\rho}-\left(\frac{2e^{\tau}\sinh^3\tau}{\cosh\tau\sinh\tau-\tau}\right)^{1/2}\vec{\phi}_0, \tag{22}$$

then

$$\xi d\theta_y dy=\frac{d\phi_y d\rho_y}{\pi D_{\mathrm{gen}}^{1/2}}\exp\left\{-\frac{1}{D_{\mathrm{gen}}}[D_{\mathrm{III}}(\phi_y^2-2\phi_y\phi_{y0}+\phi_{y0}^2e^{2\tau})-D_{\mathrm{X}}\phi_y\rho_y'-D_{\mathrm{Y}}\phi_{y0}\rho_y+D_{\mathrm{II}}\rho_y^2]\right\}, \tag{23}$$

where $D$'s and their relating functions are given in Table I. A relation

$$D_{\mathrm{X}}{}^2=4\,(D_{\mathrm{II}}D_{\mathrm{III}}-D_{\mathrm{I}}D_{\mathrm{gen}}) \tag{24}$$

satisfies among the coefficients.

The excess distribution of the path length for the projected components is derived by the inverse Laplace transforms to $\lambda$:

$$F(t,\theta_y,y,\Delta,\theta_{y0})d\theta_y dy d\Delta=\frac{d\theta_y dy d\Delta}{2\pi i}\int_{\lambda_0-\infty}^{\lambda_0+\infty}e^{\Delta\lambda}\xi(t,\theta_y,y,\lambda,\theta_{y0})d\lambda, \tag{25}$$

where the path of integration is taken parallel to the imaginary axis in the half plane of convergence of $\xi$. Likewise, the excess distribution for the spatial components can be obtained by using the folding property of the Laplace transforms:

$$\begin{aligned}A(t,\vec{\theta},\vec{r},\Delta,\vec{\theta}_0)d\vec{\theta}d\vec{r}d\Delta&=\frac{d\vec{\theta}d\vec{r}d\Delta}{2\pi i}\int e^{\Delta\lambda}\xi(t,\theta_y,y,\lambda,\theta_{y0})\\&\quad\times\xi(t,\theta_z,z,\lambda,\theta_{z0})d\lambda\\&=e^{-\tau^2u'}\frac{d\vec{\phi}d\vec{\rho}du'}{2\pi i}\int e^{u's'}\Xi_{\mathrm{gen}}(\vec{\phi},\vec{\rho},s',\vec{\phi}_0)ds'\\&\equiv\mathcal{B}(\vec{\phi},\vec{\rho},u',\vec{\phi}_0)d\vec{\phi}d\vec{\rho}du',\end{aligned} \tag{26}$$

where we introduced a nondimensional variable proportional to $\Delta$,

$$u'=\tfrac{1}{2}w_0^2\Delta/t'^2, \tag{27}$$

and rewrote the image function of the Laplace transforms in the nondimensional variables:

$$\Xi_{\mathrm{gen}}d\vec{\phi}d\vec{\rho}=\frac{d\vec{\phi}d\vec{\rho}}{\pi^2D_{\mathrm{gen}}}\exp\left\{-\frac{1}{D_{\mathrm{gen}}}[D_{\mathrm{III}}(\phi^2-2\vec{\phi}\vec{\phi}_0+\phi_0^2e^{2\tau})-D_{\mathrm{X}}\vec{\phi}\vec{\rho}'-D_{\mathrm{Y}}\vec{\phi}_0\vec{\rho}+D_{\mathrm{II}}\rho^2]\right\}. \tag{28}$$

The coefficients $D$'s depend only on $s'$ and $\tau$ as indicated in Table I [33], so we find the excess distribution of the path

TABLE II. $\Xi$'s and their abscissas of convergence. The equations to derive $\mu_{\rm I}$, $\mu_{\rm III}$, and $\mu_{\rm gen}$ are indicated in Sec. II of the text.

| Laplace transform of the distribution | | Abscissa of convergence |
|---|---|---|
| $\Xi_{\rm I}$ | $=\dfrac{1}{D_{\rm I}}$ | $-\mu_{\rm I}^2$ |
| $\Xi_{\rm II,IV}d\vec{\phi}$ | $=\dfrac{d\vec{\phi}}{\pi D_{\rm II}}\exp\left[-\dfrac{D_{\rm I}}{D_{\rm II}}\phi^2\right]$ | $-\pi^2$ |
| $\Xi_{\rm III,V}d\vec{\rho}$ | $=\dfrac{d\vec{\rho}}{\pi D_{\rm III}}\exp\left[-\dfrac{D_{\rm I}}{D_{\rm III}}\rho^2\right]$ | $-\mu_{\rm III}^2$ |
| $\Xi_{\rm gen}d\vec{\phi}d\vec{\rho}$ | $=\dfrac{d\vec{\phi}d\vec{\rho}}{\pi^2 D_{\rm gen}}\exp\left[-\dfrac{1}{D_{\rm gen}}\{D_{\rm III}(\phi^2-2\vec{\phi}\vec{\phi}_0+\phi_0^2e^{2\tau})-D_{\rm X}\vec{\phi}\vec{\rho}'-D_{\rm Y}\vec{\phi}_0\vec{\rho}+D_{\rm II}\rho^2\}\right]$ | $-\mu_{\rm gen}^2$ |

length represented in $u'$ is the function of only $\tau$ or the fraction of residual energy $E/E_0$, not depending on $E_0$, $E$, $t$, or $\epsilon$ explicitly, if we measure the deflection angle and the lateral displacement by those root mean square values as defined in Eqs. (19)–(22). It can be easily confirmed that limiting the value of $\Xi_{\rm gen}$ as $\tau\to 0$ gives the solution of the Yang equation without ionization in the image space of the Laplace transforms, obtained in PP.

The Laplace transforms of the excess-path-length distribution for the respective geometrical conditions, indicated in Table I of PP, are obtained by integrating the image function for case gen, $\Xi_{\rm gen}$, over $\vec{\phi}$ and/or $\vec{\rho}$ with $\theta_0=0$: that with $\vec{\theta}$ and $\vec{r}$ integrated (case I), that with $\vec{r}$ integrated and $\vec{\theta}$ fixed (case IV) or fixed to 0 (case II), and that with $\vec{\theta}$ integrated and $\vec{r}$ fixed (case V) or fixed to 0 (case III). These $\Xi$'s are listed in Table II together with their abscissas of convergence, where $\mu_{\rm I}$, $\mu_{\rm III}$, and $\mu_{\rm gen}$ are the smallest positive solutions to satisfy

$$\mu_{\rm I}\cot\mu_{\rm I}+\tau=0, \tag{29}$$

$$\mu_{\rm III}\cot\mu_{\rm III}-\tau\coth\tau=0, \tag{30}$$

and

$$2-2\cosh\tau\cos\mu_{\rm gen}-(\tau^{-1}\mu_{\rm gen}-\mu_{\rm gen}{}^{-1}\tau)\sinh\tau\sin\mu_{\rm gen}=0, \tag{31}$$

respectively.

## III. CALCULATION OF THE EXCESS-PATH-LENGTH DISTRIBUTION

We will show the joint distributions of the excess path length under the respective geometrical conditions by applying inverse Laplace transforms to $\Xi$'s.

### A. Case I

$$\begin{aligned}\Xi_{\rm I}&=(\cosh\sqrt{s'}+\tau\sinh\sqrt{s'}/\sqrt{s'})^{-1}e^{\tau}\\&=\frac{2e^{\tau}\sqrt{s'}}{(\sqrt{s'}+\tau)e^{\sqrt{s'}}+(\sqrt{s'}-\tau)e^{-\sqrt{s'}}}\\&=\frac{2e^{\tau}}{\sqrt{s'}+\tau}\sqrt{s'}e^{-\sqrt{s'}}-\frac{2e^{\tau}}{(\sqrt{s'}+\tau)^2}\\&\quad\times(s'-\tau\sqrt{s'})e^{-3\sqrt{s'}}+\cdots.\end{aligned} \tag{32}$$

Thus using the formulas indicated in Appendix C we have

$$\begin{aligned}\mathcal{B}_{\rm I}(u')&=\frac{2}{\sqrt{\pi u'}}\left(-\tau+\frac{1}{2u'}\right)e^{\tau-\tau^2u'-1/(4u')}\\&\quad+2\tau^2e^{2\tau}\,\mathrm{erfc}\left(\frac{1}{2\sqrt{u'}}+\tau\sqrt{u'}\right)\\&\quad+\frac{4\tau^3}{\sqrt{\pi/u'}}\left(2+\frac{3}{2\tau^2u'}-\frac{3}{4\tau^3u'^2}\right)\\&\quad\times e^{\tau-\tau^2u'-9/(4u')}-2\tau^3\left(4\tau u'+6+\frac{5}{\tau}\right)e^{4\tau}\\&\quad\times\mathrm{erfc}\left(\frac{3}{2\sqrt{u'}}+\tau\sqrt{u'}\right)+\cdots.\end{aligned} \tag{33}$$

By taking the asymptotic approximations, good to within 1%,

$$\mathcal{B}_{\mathrm{I}}(u')=\begin{cases}\dfrac{2}{\sqrt{\pi u'}}\left(-\tau+\dfrac{1}{2u'}\right)e^{\tau-\tau^2u'-1/(4u')}+2\tau^2e^{2\tau}\,\mathrm{erfc}\left(\dfrac{1}{2\sqrt{u'}}+\tau\sqrt{u'}\right) & \text{for}\quad u'\leqslant 0.3,\\ \dfrac{2\mu_{\mathrm{I}}^2\,\sin\,\mu_{\mathrm{I}}}{\mu_{\mathrm{I}}-\cos\,\mu_{\mathrm{I}}\sin\,\mu_{\mathrm{I}}}e^{\tau-(\tau^2+\mu_{\mathrm{I}}^2)u'} & \text{for}\quad u'\geqslant 0.3,\end{cases}\tag{34}$$

where $\mu_{\mathrm{I}}$ is defined in Eq. (29).

### B. Case II

$$\Xi_{\mathrm{II}}d\vec{\phi}=\frac{d\vec{\phi}}{\pi}\,\frac{\sinh\,\tau/\tau}{\sinh\sqrt{s'}/\sqrt{s'}}=\frac{2\sinh\,\tau d\vec{\phi}}{\pi\tau}[\,\sqrt{s'}e^{-\sqrt{s'}}+\sqrt{s'}e^{-3\sqrt{s'}}+\cdots].\tag{35}$$

Thus using the formulas indicated in Appendix C we have

$$\mathcal{B}_{\mathrm{II}}(u')d\vec{\phi}=\frac{\sinh\,\tau d\vec{\phi}}{\tau\sqrt{\pi^3u'^3}}e^{-\tau^2u'}\left[\left(\frac{1}{2u'}-1\right)e^{-1/(4u')}+\left(\frac{9}{2u'}-1\right)e^{-9/(4u')}+\cdots\right].\tag{36}$$

By taking the asymptotic approximations, good to within 1%,

$$\mathcal{B}_{\mathrm{II}}(u')d\vec{\phi}=\begin{cases}\dfrac{\tau^{-1}\,\sinh\,\tau}{\sqrt{\pi^3u'^3}}\left(\dfrac{1}{2u'}-1\right)e^{-\tau^2u'-1/(4u')}d\vec{\phi} & \text{for}\quad u'\leqslant 0.4,\\ 2\pi\tau^{-1}\,\sinh\,\tau e^{-(\tau^2+\pi^2)u'}d\vec{\phi} & \text{for}\quad u'\geqslant 0.4.\end{cases}\tag{37}$$

### C. Case III

$$\begin{aligned}\Xi_{\mathrm{III}}d\vec{\rho}&=\frac{d\vec{\rho}}{2\pi}\,\frac{(\cosh\,\tau\sinh\,\tau-\tau)(\tau^{-2}s'-1)}{\sinh\,\tau\cosh\sqrt{s'}-\tau\cosh\,\tau\sinh\sqrt{s'}/\sqrt{s'}}\\&=\frac{(\cosh\,\tau\sinh\,\tau-\tau)d\vec{\rho}}{\pi\tau^2\,\sinh\,\tau}\left\{\frac{s'-\tau^2}{\sqrt{s'}-\tau\coth\,\tau}\sqrt{s'}e^{-\sqrt{s'}}-\left[\frac{s'-\tau^2}{\sqrt{s'}-\tau\coth\,\tau}+\frac{2\tau(s'-\tau^2)\coth\,\tau}{(\sqrt{s'}-\tau\coth\,\tau)^2}\right]\sqrt{s'}e^{-3\sqrt{s'}}+\cdots\right\}.\end{aligned}\tag{38}$$

Thus using the formulas indicated in Appendix C we have

$$\begin{aligned}\mathcal{B}_{\mathrm{III}}(u')d\vec{\rho}=\frac{\cosh\,\tau\sinh\,\tau-\tau}{\tau^2\,\sinh\,\tau\sqrt{\pi^3u'}}e^{-\tau^2u'}d\vec{\rho}\Bigg\{&\left[\frac{\tau^3\,\cosh\,\tau}{\sinh^3\,\tau}-\frac{\tau(\cosh\,\tau\sinh\,\tau-\tau)}{2u'\,\sinh^2\,\tau}+\frac{\tau\coth\,\tau-3}{4u'^2}+\frac{1}{8u'^3}\right]e^{-1/(4u')}\\&+\frac{\tau^4\,\cosh^2\,\tau}{\sinh^4\,\tau}e^{\tau^2u'\coth^2\tau-\tau\coth\tau}\,\mathrm{erfc}\left(\frac{1}{2\sqrt{u'}}-\tau\sqrt{u'}\coth\,\tau\right)-\left[\frac{4\tau^5\,\cosh^3\,\tau}{\sinh^5\,\tau}+\frac{7\tau^3\,\coth^3\,\tau-3\tau^3\,\coth\,\tau}{u'}\right.\\&\left.+\frac{15\tau^2\,\coth^2\,\tau-3\tau\coth\,\tau-3\tau^2}{2u'^2}+\frac{27\tau\coth\,\tau-9}{4u'^3}+\frac{27}{8u'^4}\right]u'e^{-9/(4u')}-\left[\frac{4\tau^6u'\,\cosh^4\,\tau}{\sinh^6\,\tau}-\frac{6\tau^5\,\cosh^3\,\tau}{\sinh^5\,\tau}\right.\\&\left.+9\tau^4\,\coth^4\,\tau-5\tau^4\,\coth^2\,\tau\right]e^{\tau^2u'\coth^2\tau-3\tau\coth\tau}\,\mathrm{erfc}\left(\frac{3}{2\sqrt{u'}}-\tau\sqrt{u'}\coth\,\tau\right)+\cdots\Bigg\}.\end{aligned}\tag{39}$$

By taking the asymptotic approximations, good to within 1%,

$$\mathcal{B}_{\mathrm{III}}(u')d\vec{\rho}=\begin{cases}\left[\left(\dfrac{\tau^3\cosh\tau}{\sinh^3\tau}-\dfrac{\tau(\cosh\tau\sinh\tau-\tau)}{2u'\sinh^2\tau}+\dfrac{\tau\coth\tau-3}{4u'^2}+\dfrac{1}{8u'^3}\right)e^{-1/(4u')}\right. & \\ \left.+\dfrac{\tau^4\cosh^2\tau}{\sinh^4\tau}e^{\tau^2u'\coth^2\tau-\tau\coth\tau}\,\mathrm{erfc}\left(\dfrac{1}{2\sqrt{u'}}-\tau\sqrt{u'}\coth\tau\right)\right]\dfrac{\cosh\tau\sinh\tau-\tau}{\tau^2\sinh\tau\sqrt{\pi^3u'}}e^{-\tau^2u'}d\vec{\rho} & \text{for}\quad u'\leqslant 0.15,\\ \dfrac{-(\tau^2+\mu_{\mathrm{III}}^2)(\cosh\tau\sinh\tau-\tau)\mu_{\mathrm{III}}^2\sin\mu_{\mathrm{III}}}{\pi(\mu_{\mathrm{III}}-\cos\mu_{\mathrm{III}}\sin\mu_{\mathrm{III}})\tau^2\sinh\tau}e^{-(\tau^2+\mu_{\mathrm{III}}^2)u'}d\vec{\rho} & \text{for}\quad u'\geqslant 0.15,\end{cases} \tag{40}$$

where $\mu_{\mathrm{III}}$ is defined in Eq. (30).

### D. Cases IV, V, and gen

Image functions have essential singularities in cases of IV, V, and gen, as PP. In those cases we can obtain the distributions asymptotically with the saddle point method:

$$\mathcal{B}(u')du'=e^{-\tau^2u'}\frac{du'}{2\pi i}\int e^{u's'}\,\Xi(s')ds'$$

$$\cong[2\pi(\partial^2/\partial s'^2)\ln\Xi(\bar{s'})]^{-1/2}\,\Xi(\bar{s'})e^{-(\tau^2-\bar{s'})u'}du', \tag{41}$$

where

$$u'=-(\partial/\partial s')\ln\Xi(\bar{s'}). \tag{42}$$

The saddle point $\bar{s'}$ is taken on the real axis at the right-hand side of the abscissa of convergence indicated in Table II.

### E. Moments and statistical values

Zeroth moment, that is, integration of the distribution with respect to the excess of the path length can be obtained by limiting the value of $\xi$ as $s'\to\tau^2$:

$$\lim_{s'\to\tau^2}\xi d\theta_y dy=\frac{1}{\pi}\left[\frac{2(\cosh\tau\sinh\tau-\tau)e^{-\tau}\sinh\tau}{\sinh^2\tau-\tau^2}\right]^{1/2}d\phi_y d\rho_y$$

$$\times\exp\left\{-\frac{2(\cosh\tau\sinh\tau-\tau)e^{-\tau}\sinh\tau}{\sinh^2\tau-\tau^2}\left[\phi_y'^2-\frac{2(\tau-e^{-\tau}\sinh\tau)\phi_y'\rho_y'}{[2(\cosh\tau\sinh\tau-\tau)e^{-\tau}\sinh\tau]^{1/2}}+\rho_y'^2\right]\right\}. \tag{43}$$

This solution gives the Fermi distribution of the multiple Coulomb scattering indicating the joint distribution of deflection angle and lateral displacement with a finite incident angle $\theta_{y0}$, taking into account the ionization loss. The solution with $\theta_{y0}=0$, which changes $\phi_y'$ and $\rho_y'$ to $\phi_y$ and $\rho_y$, gives Eyges' solution regarding his $W(t)$ as our Eq. (2). This fact means that the Fermi solution with a finite incident angle can be obtained by simple replacements, $\vec{\theta}$ and $\vec{r}$, in the solution for normal incidence with $\vec{\theta}-\vec{\theta}_0$ and $\vec{r}-\vec{\theta}_0 t$.

Equation (43) gives the covariant value between $\vec{\phi}'$ and $\vec{\rho}'$, which is identical with the correlation coefficient between the projected components, $\theta_y'$ and $y'$:

$$\langle\vec{\phi}'\vec{\rho}'\rangle_{\mathrm{av}}=\frac{\langle\theta_y'y'\rangle_{\mathrm{av}}}{\langle\theta_y'^2\rangle_{\mathrm{av}}^{1/2}\langle y'^2\rangle_{\mathrm{av}}^{1/2}}=\frac{\tau-e^{-\tau}\sinh\tau}{[2(\cosh\tau\sinh\tau-\tau)e^{-\tau}\sinh\tau]^{1/2}}. \tag{44}$$

This value was a constant, $\sqrt{3}/2$, irrespective of traversed thickness in the case of no ionization loss [6,9], but this time it decreases gradually from $\sqrt{3}/2$ with loss of energy and rapidly falls to 0 just before they dissipate their whole energies, reflecting the decrease of correlation between them.

From the limiting values as $s'\to\tau^2$ of the first and the second logarithmic derivatives of $\Xi(s')$'s, we get the means and the variances of the excess-path-length distribution for the respective cases:

TABLE III. Mean values of excess-path length distribution.

| Case | $\langle u' \rangle_{\rm av}$ |
|---|---|
| I | $\frac{1}{2\tau^2}\{-e^{-\tau}\sinh\tau+\tau\}$ |
| II,IV | $\frac{-\sinh\tau+\tau\cosh\tau}{2\tau^2\sinh\tau}+\frac{\phi^2 e^{-\tau}}{2\tau^2\sinh\tau}\{\cosh\tau\sinh\tau-\tau\}$ |
| III,V | $\frac{-3\cosh\tau\sinh\tau+\tau(3\cosh^2\tau-\sinh^2\tau)}{4\tau^2(\cosh\tau\sinh\tau-\tau)}$ $+\frac{\rho^2 e^{-\tau}}{4\tau^2(\cosh\tau\sinh\tau-\tau)}\{\cosh\tau\sinh\tau(3\cosh\tau+\sinh\tau)-\tau(3\cosh\tau-\sinh\tau)-2\tau^2 e^{\tau}\}$ |
| gen | $\frac{-2\sinh^2\tau+\tau\cosh\tau\sinh\tau+\tau^2}{2\tau^2(\sinh^2\tau-\tau^2)}$ $+\frac{(\phi^2-2\vec{\phi}\vec{\phi}_0+\phi_0^2 e^{2\tau})e^{-\tau}\sinh\tau}{2\tau^2(\sinh^2\tau-\tau^2)^2}$ $\times\{\cosh\tau\sinh^3\tau-3\tau\sinh^2\tau+3\tau^2\cosh\tau\sinh\tau-\tau^3(\cosh^2\tau+\sinh^2\tau)\}$ $-\frac{\vec{\phi}\vec{\rho}'\sqrt{(\cosh\tau\sinh\tau-\tau)e^{-\tau}\sinh\tau}}{\sqrt{2}\tau^2(\sinh^2\tau-\tau^2)^2}$ $\times\{-e^{-\tau}\sinh^3\tau+3\tau\sinh^2\tau-\tau^2\sinh\tau(3\cosh\tau-2\sinh\tau)+\tau^3 e^{-2\tau}-\tau^4\}$ $-\frac{\vec{\phi}_0\vec{\rho}\sqrt{(\cosh\tau\sinh\tau-\tau)e^{-\tau}\sinh\tau}}{\sqrt{2}\tau^2(\sinh^2\tau-\tau^2)^2}$ $\times\{e^{\tau}\sinh^3\tau-3\tau\sinh^2\tau+\tau^2\sinh\tau(3\cosh\tau+2\sinh\tau)-\tau^3 e^{2\tau}-\tau^4\}$ $+\frac{\rho^2 e^{-\tau}(\cosh\tau\sinh\tau-\tau)}{\tau^2(\sinh^2\tau-\tau^2)^2}\{\sinh^3\tau-\tau^3\cosh\tau\}$ |

$$\langle u' \rangle_{\rm av} = -\lim_{s'\to\tau^2} (\partial/\partial s')\ln \Xi(s'), \tag{45}$$

and

$$\langle u'^2 \rangle_{\rm av} - \langle u' \rangle_{\rm av}^2 = \lim_{s'\to\tau^2} (\partial^2/\partial s'^2)\ln \Xi(s'). \tag{46}$$

Results are shown in Tables III and IV.

## IV. THE EXCESS DISTRIBUTION OF THE PATH LENGTH AND THE EFFECTS OF TAKING INTO ACCOUNT IONIZATION LOSS

We discuss the excess distribution of the path length for the respective geometrical conditions. In order to discuss the effect of ionization loss and compare results with those without ionization obtained in PP, it may be better to represent the excess path length by $u$ defined in PP:

$$u = \tfrac{1}{2} w_0^2 \Delta / t^2. \tag{47}$$

Thus the distribution becomes

$$A(\Delta)d\Delta = B(u)du = (\tau^{-1}e^{-\tau}\sinh\tau)^2 \mathcal{B}((\tau^{-1}e^{-\tau}\sinh\tau)^2 u)du. \tag{48}$$

It can be easily understood that the probability density $B(u)$'s for the respective cases also are the functions of only $\tau$, or $E/E_0$, if we describe the deflection angle and lateral displacement in units of their root mean square values, as $\mathcal{B}(u')$'s are.

The probability densities, $B_1(u)$'s, for charged particles having traversed the fractional thickness $t/R$ of 0.25, 0.50, and 0.75 in the material and having dissipated the same fraction of energy to $E_0$ are shown in Fig. 1 [34]. The result without ionization obtained in PP is also shown as $t/R=0$. The more the fraction of traversed thickness $t/R$ increases, the more the distributions move to the larger ward of excess

TABLE IV. Variances of excess-path length distribution.

| Case | $\langle u'^2\rangle_{\rm av}-\langle u'\rangle_{\rm av}^2$ |
|---|---|
| I | $\frac{e^{-\tau}}{4\tau^4}\{-e^{-\tau}\sinh\tau(3\cosh\tau+2\sinh\tau)+\tau(3\cosh\tau-\sinh\tau)\}$ |
| II,IV | $\frac{-2\sinh^2\tau+\tau\cosh\tau\sinh\tau+\tau^2}{4\tau^4\sinh^2\tau}+\frac{\phi^2e^{-\tau}}{4\tau^4\sinh^2\tau}\{\cosh\tau\sinh^2\tau+\tau\sinh\tau-2\tau^2\cosh\tau\}$ |
| III,V | $\frac{1}{48\tau^4(\cosh\tau\sinh\tau-\tau)^2}\{-33\cosh^2\tau\sinh^2\tau+6\tau\cosh\tau\sinh\tau(11\cosh^2\tau-9\sinh^2\tau)$ $-3\tau^2e^{-\tau}(11\cosh\tau-3\sinh\tau)+16\tau^3\cosh\tau\sinh\tau-4\tau^4\}$ $+\frac{\rho^2}{24\tau^4(\cosh\tau\sinh\tau-\tau)^2}\{3\cosh^2\tau\sinh^2\tau-6\tau\cosh\tau\sinh\tau$ $+3\tau^2(\cosh^2\tau+3\sinh^2\tau)-8\tau^3\cosh\tau\sinh\tau-4\tau^4\}$ |
| gen | $\frac{1}{24\tau^4(\sinh^2\tau-\tau^2)^2}\{-21\sinh^4\tau+6\tau\cosh\tau\sinh^3\tau+42\tau^2\sinh^2\tau$ $-18\tau^3\cosh\tau\sinh\tau-\tau^4(9\cosh^2\tau-16\sinh^2\tau)-\tau^6\}$ $+\frac{(\phi^2-2\vec{\phi}\vec{\phi}_0+\phi_0^2e^{2\tau})e^{-\tau}\sinh\tau}{12\tau^4(\sinh^2\tau-\tau^2)^3}\{3\cosh\tau\sinh^5\tau-3\tau\sinh^4\tau-18\tau^2\cosh\tau\sinh^3\tau$ $+2\tau^3\sinh^2\tau(21\cosh^2\tau-11\sinh^2\tau)-\tau^4\cosh\tau\sinh\tau(33\cosh^2\tau-26\sinh^2\tau)$ $+3\tau^5(3\cosh^2\tau+2\sinh^2\tau)-5\tau^6\cosh\tau\sinh\tau+\tau^7\}$ $-\frac{\vec{\phi}\vec{\rho}'\sqrt{(\cosh\tau\sinh\tau-\tau)e^{-\tau}\sinh\tau}}{6\sqrt{2}\tau^4(\sinh^2\tau-\tau^2)^3}\{-3e^{-\tau}\sinh^5\tau+3\tau\sinh^4\tau$ $+6\tau^2\sinh^3\tau(3\cosh\tau-2\sinh\tau)-2\tau^3\sinh^2\tau(21\cosh^2\tau-9\cosh\tau\sinh\tau-11\sinh^2\tau)$ $+\tau^4e^{-\tau}\sinh\tau(33\cosh^2\tau+18\cosh\tau\sinh\tau-8\sinh^2\tau)$ $-3\tau^5(3\cosh^2\tau-2\cosh\tau\sinh\tau+2\sinh^2\tau)+5\tau^6e^{-\tau}\sinh\tau-\tau^7\}$ $-\frac{\vec{\phi}_0\vec{\rho}\sqrt{(\cosh\tau\sinh\tau-\tau)e^{-\tau}\sinh\tau}}{6\sqrt{2}\tau^4(\sinh^2\tau-\tau^2)^3}\{3e^{\tau}\sinh^5\tau-3\tau\sinh^4\tau$ $-6\tau^2\sinh^3\tau(3\cosh\tau+2\sinh\tau)+2\tau^3\sinh^2\tau(21\cosh^2\tau+9\cosh\tau\sinh\tau-11\sinh^2\tau)$ $-\tau^4e^{\tau}\sinh\tau(33\cosh^2\tau-18\cosh\tau\sinh\tau-8\sinh^2\tau)$ $+3\tau^5(3\cosh^2\tau+2\cosh\tau\sinh\tau+2\sinh^2\tau)-5\tau^6e^{\tau}\sinh\tau+\tau^7\}$ $+\frac{\rho^2e^{-\tau}(\cosh\tau\sinh\tau-\tau)}{12\tau^4(\sinh^2\tau-\tau^2)^3}\{3\sinh^5\tau-12\tau^2\sinh^3\tau+18\tau^3\cosh\tau\sinh^2\tau$ $-\tau^4\sinh\tau(15\cosh^2\tau-8\sinh^2\tau)+6\tau^5\cosh\tau-5\tau^6\sinh\tau\}$ |

path length increasing their widths, even at the same traversed thickness $t$ depending on the difference of materials through $\varepsilon$.

The probability densities for case II, IV, case III, V, and case gen are indicated in Figs. 2–4, respectively, corresponding to their fractional thicknesses $t/R$ of 0.25 and 0.50. They can be compared with the results not taking into account ionization loss ($t/R=0$), derived in PP.

The results obtained exactly by the series expansion and asymptotically by the saddle point method are compared in Fig. 2 and Fig. 3 for case II and case III, respectively: the exact ones in the solid line and the asymptotic ones in the dotted line. The asymptotic approximation by the saddle point method shows good accuracy in these cases.

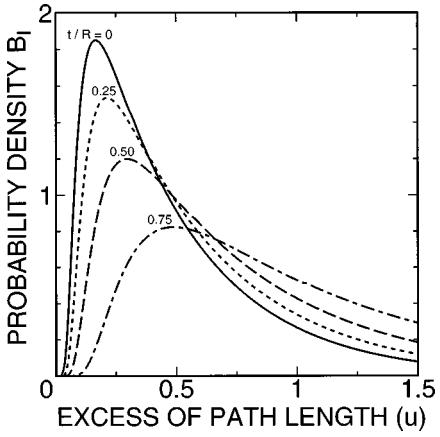


FIG. 1. Excess distributions of path length in case I at various fractional thicknesses $t/R$, without the ionization loss ($t/R=0$). Abscissa means $\Delta/(2t^2/w_0^2)$ or the excess-path length measured in units of twice of $\langle\Delta_I\rangle_{av}$ predicted without the ionization loss.

In case V and gen, the distributions have the starting points $u_G$'s depending on the lateral displacement $\rho$:

$$u_G=(t'/t)^2 \lim_{s'\to\infty} u'=\tfrac{1}{2}(\cosh\tau\sinh\tau-\tau)\rho^2 e^{\tau}\sinh^{-3}\tau. \tag{49}$$

They agree with the geometrical difference between the chord length [13] and the thickness of the material, $r^2/(2t)$, under the small angle approximation, same as PP. Mean excess $\langle u'\rangle_{av}$ of case V, shown in Table III, includes this geometrical excess in the value. Figure 5 shows the fraction of *pure* scattering excess or the excess excluding the geometrical one to the total, $(\langle u_V\rangle_{av}-u_G)/\langle u_V\rangle_{av}$, against the lateral displacement measured in its root mean square value predicted without ionization loss, $r/r_{rms}$ with $r_{rms}=2t^{3/2}/(\sqrt{3}w_0)$. In the region of small lateral displacement ($r/r_{rms}\ll 1$), where the existence probability of the particle is extremely high, the pure multiple scattering contributes much dominantly to the excess of the path length. The fraction decreases gradually with increase of $r/r_{rms}$, and reaches to some finite value as $r/r_{rms}\to\infty$, depending on the fractional thickness $t/R$. The limiting value, having taken $\frac{1}{6}$ in case without ionization loss, increases gradually with the fractional thickness and reaches to $\frac{1}{2}$ with dissipation of their

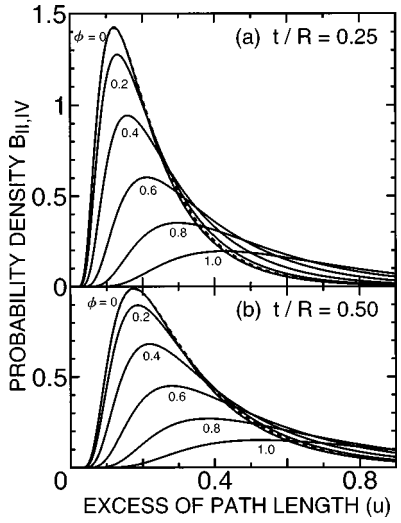


FIG. 2. Excess distributions of path length in cases II and IV at the fractional thicknesses of (a) 0.25 and (b) 0.50. The parameter $\phi$ shows the deflection angle measured in its root mean square value. The distribution in case II obtained by the saddle point method is indicated together in the dotted line.

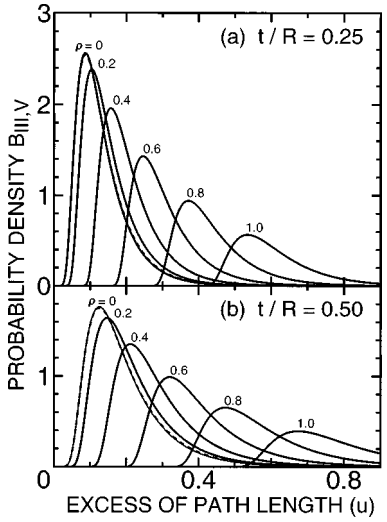


FIG. 3. Excess distributions of path length in cases III and V at the fractional thicknesses of (a) 0.25 and (b) 0.50. The parameter $\rho$ shows the lateral displacement measured in its root mean square value. The distribution in case III obtained by the saddle point method is indicated together in the dotted line.

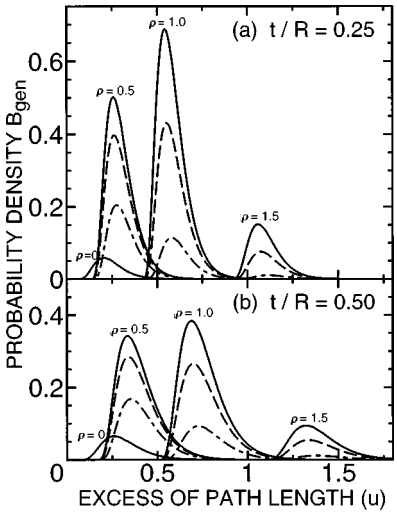


FIG. 4. Excess distributions of path length in case gen at the fractional thicknesses of (a) 0.25 and (b) 0.50. In the figure, the incident angle is fixed to 0 ($\phi_0=0$), and the absolute value of the nondimensional deflection angle is fixed to 1 ($\phi=1$) and that of the nondimensional lateral displacement is distinguished by the parameter $\rho$, where the angles between $\vec{\phi}$ and $\vec{\rho}$ are 0 (solid line), $\frac{1}{8}\pi$ (dashed line), and $\frac{1}{4}\pi$ (dot-dashed line).

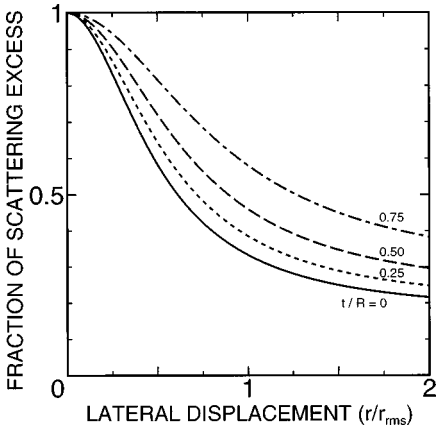


FIG. 5. Fraction of the pure multiple scattering excess, excluding the geometrical excess, at various fractional thicknesses. Abscissa means lateral displacement measured in its root mean square value predicted without ionization loss.

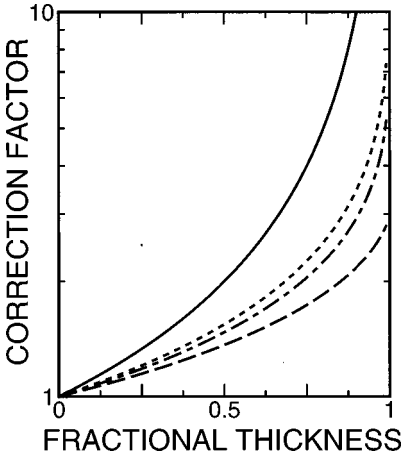


FIG. 6. Correction factors by taking into account ionization loss, to the mean squares of deflection angle (solid line) and lateral displacement (dashed line), and to the mean excess (dot line) and the square root of variance (dot-dashed line) of path length.

whole energies. This fact shows that the excess of the path length due to the pure multiple Coulomb scattering becomes more and more important than the geometrical excess when we take into account the ionization loss in propagation of charged particles.

Table V shows the mean square deflection angle, lateral displacement, and the mean and the variance of the excess path length averaged over all normally-incident particles (case I), before taking into account the ionization loss and after, together with the correction factors defined by the ratios of the latter to the former. Without the ionization loss, $\langle\theta^2\rangle_{\rm av}$, $\langle r^2\rangle_{\rm av}$, and $\langle\Delta\rangle_{\rm av}$ increased linearly, cubically, and quadratically with $t$. On the other hand, after receiving the ionization loss, they are corrected additively by factors depending only on fractional thickness $t/R$ or fraction of dissipated energy $(E_0-E)/E_0$, not explicitly depending on traversed thickness $t$ nor difference of materials through $\varepsilon$, as shown in Fig. 6.

The influence of the fluctuation of the excess path length on the energy-loss distribution of charged particles, discussed in PP, increases still more with increase of the fractional thickness due to increase of the correction factor indicated above, when we take into account the ionization loss.

At the limit for charged particles to reach to the maximum thickness $R$, $\langle\theta^2\rangle_{\rm av}$ diverges, and $\langle r^2\rangle_{\rm av}$ reaches to the finite value, 3 times that of the predicted result without the ionization loss. $\langle\Delta\rangle_{\rm av}$ diverges logarithmically on the other hand. The divergence of mean excess path lengths with dissipation of their whole energies leads to a contradiction and shows the limit of applicability of our present theory, because the charged particles have to dissipate infinite energies proportional to their path lengths. The divergence does not come from our approximation, $w=2E/E_s$ instead of $w=2pv/E_s$, nor from the Gaussian approximation neglecting the higher moments of the single scattering formula [12,6]. It

TABLE V. Comparison of mean values and a variance $\sigma_\Delta^2=\langle\Delta^2\rangle_{\rm av}-\langle\Delta\rangle_{\rm av}^2$ before taking into account ionization loss and after.

| | $\varepsilon=0$ | with ionization | correction factor |
|---|---|---|---|
| $\langle\theta^2\rangle_{\rm av}$ | $\frac{4}{w_0^2}t$ | $\frac{4t}{w_0^2}\frac{E_0}{E}$ | $\frac{E_0}{E}$ |
| $\langle r^2\rangle_{\rm av}$ | $\frac{4}{3w_0^2}t^3$ | $\frac{4E_0^3}{w_0^2\varepsilon^3}\frac{E}{E_0}\left\{\frac{E_0}{E}-\frac{E}{E_0}+2\ln\frac{E}{E_0}\right\}$ | $\frac{3}{(1-E/E_0)^3}\frac{E}{E_0}\left\{\frac{E_0}{E}-\frac{E}{E_0}+2\ln\frac{E}{E_0}\right\}$ |
| $\langle\Delta\rangle_{\rm av}$ | $\frac{1}{w_0^2}t^2$ | $\frac{-2E_0^2}{w_0^2\varepsilon^2}\left\{1-\frac{E}{E_0}+\ln\frac{E}{E_0}\right\}$ | $\frac{-2}{(1-E/E_0)^2}\left\{1-\frac{E}{E_0}+\ln\frac{E}{E_0}\right\}$ |
| $\sigma_\Delta^2$ | $\frac{2}{3w_0^4}t^4$ | $\frac{-4E_0^4}{w_0^4\varepsilon^4}\left\{\left(1-\frac{E}{E_0}\right)\left(5+\frac{E}{E_0}\right)\right.$ | $\frac{-6}{(1-E/E_0)^4}\left\{\left(1-\frac{E}{E_0}\right)\left(5+\frac{E}{E_0}\right)\right.$ |
| | | $\left.+4\left(\frac{1}{2}+\frac{E}{E_0}\right)\ln\frac{E}{E_0}\right\}$ | $\left.+4\left(\frac{1}{2}+\frac{E}{E_0}\right)\ln\frac{E}{E_0}\right\}$ |

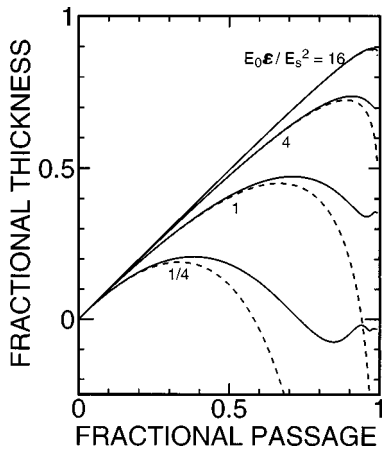


FIG. 7. Mean fractional thicknesses of path length $\langle t\rangle_{\rm av}/R$ for various incident energies evaluated more accurately than the small angle approximation for assumed particles traversing with the mean square deflection angle (solid line), together with those under the small angle approximation (dot line). Abscissa means $s/R$.

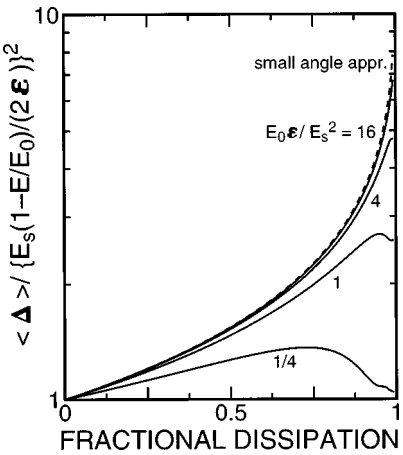


FIG. 8. Mean excesses of path length for various incident energies evaluated more accurately than the small angle approximation (solid lines), together with the mean excess evaluated with the small angle approximation (dot line). Abscissa means $s/R$ for the former and $t/R$ for the latter, both indicating the fraction of dissipated energy.

comes strictly from violations to the small angle approximation [3]. To solve this problem, we have to improve the multiple scattering theory more accurately than the small angle approximation.

Introducing the variable $s$ for the actual path length as done by Scott [13] and measuring the path length along the trajectory itself as noted by Rossi [18], we tried a more accurate evaluation of mean values than that through the small angle approximation: for mean thickness $\langle t\rangle_{\rm av}$ of traverse and mean excess $\langle\Delta\rangle_{\rm av}$ of the path length averaged over the all normally-incident particles (case I) in Appendix B, neglecting the fluctuation of $\theta^2$. The mean thicknesses defined by the projections of the actual path length onto the initial direction of the incident particle are shown in Fig. 7 for several incident-energy parameters, $E_0\varepsilon/E_s^2$, together with those under the small angle approximation. They might be observed in visible detectors as the contracted thicknesses of traverse due to the multiple Coulomb scattering. The mean excesses defined by the differences between the actual path length and the mean thickness are indicated in Fig. 8 for those parameters, together with the result predicted through the small angle approximation which does not depend on $E_0\varepsilon/E_s^2$. The comparison indicates that the mean excess derived from the small angle approximation, $1-\frac{1}{2}\theta^2$ instead of $\cos\theta$, has high accuracy when the incident energy $E_0$ is larger than $E_s^2/\varepsilon$ or the traversed thickness $t$ is smaller enough than the range $R$.

$s$, $t$, and $\Delta$ defined above are identical with $s$, $x$, and $u$ in Scott formulation [13]. But it should be noticed that under our assumption of ionization loss proportional to $s$, the average of Scott's deficiency of the path length defined by $\langle u\rangle_{\rm av}=s-\langle x\rangle_{\rm av}$ also diverges at the limit of dissipation of their whole energies due to the small angle approximation, so that the average of traversed thickness, $\langle x\rangle_{\rm av}$, diverges instead toward backward direction.

These divergences are caused by the infinite increase of approximated term, $1-\frac{1}{2}\theta^2$ in place of oscillating $\cos\theta$, at large angles of $\theta^2\gg 2$. The divergence is so weak that another approximation, $(1+\frac{1}{2}\theta^2)^{-1}$ in place of $\cos\theta$ by the small angle approximation, gives no more divergence to the average of $\Delta$, as shown in Appendix B. But we can confirm that the accuracy of the result is not improved by the new approximation.

## V. CONCLUSION

The diffusion equation of Yang to describe the longitudinal distribution of fast charged particles under the multiple Coulomb scattering process has been improved to take into account continuous energy loss by ionization and the equation has been completely solved in the image space of Laplace transforms under the most generalized conditions of geometry (in Tables I and II). Applying the inverse Laplace transforms, we have obtained the excess distributions of the path length exactly in series expansion (cases I–III) and asymptotically in the saddle point method (cases IV, V, and gen). The distributions corresponding to the respective geometrical conditions are shown in Figs. 1–4, together with their means and variances in Tables III and IV.

Contributions to the mean excess of the path length are compared between the two exclusive factors, the pure multiple-scattering excess and the geometrical excess. We have confirmed in Fig. 5 that the contribution from the former is dominant at the smaller distance from the incident axis where the charged particles traverse in extremely high probability, and the fraction increases much with dissipation of their energies.

The correction factors by taking into account the ionization loss to those obtained in PP are evaluated for mean square deflection angles, lateral displacements, and mean and variance of the excess path length averaged over all the normally-incident particles (Table V and Fig. 6). The restrictions for the present result due to the small angle approximation are also discussed (Figs. 7 and 8).

Although there exist limits of applicability caused by the

Gaussian approximation and the small angle approximation, the present investigations for the process of multiple Coulomb scattering will be very useful in predicting stochastic properties of fast charged particles traversing through materials if we take much care about the effects of single and plural scatterings discussed in PP and the restrictions from the small angle approximation discussed in this paper.


## ACKNOWLEDGMENTS

The author wishes to express his thanks to Professor T. Kitamura, Doctor S. Dake, and Doctor S. Tanaka for useful discussions about the contents. A part of this work was done at Research Center for Information Sciences of Nagoya Women's University.


## APPENDIX A: MEAN VALUES OF DISTRIBUTION IN MULTIPLE SCATTERING PROCESS

We can obtain mean square deflection angle and lateral displacement as well as mean excess of the path length averaged over all the normally-incident particles (case I) by directly integrating our basic equation (1). We can remove the last term on the left hand side of Eq. (1) by taking into account the dependence of $E$ on $t$. Multiplying $\theta^2$, $\theta y$, and $y^2$ on both sides of the equation, respectively, and integrating over $\theta$, $y$, and $\Delta$, we get differential equations for the respective mean values for projected component to the $t$-$y$ plane:

$$\frac{d}{dt}\langle \theta_y^2\rangle_{\rm av}=\frac{2}{w^2(t)}, \tag{A1}$$

$$\frac{d}{dt}\langle \theta_y y\rangle_{\rm av}=\langle \theta_y^2\rangle_{\rm av}, \tag{A2}$$

$$\frac{d}{dt}\langle y^2\rangle_{\rm av}=2\langle \theta_y y\rangle_{\rm av}. \tag{A3}$$

Thus

$$\langle \theta_y^2\rangle_{\rm av}=\int_0^t \frac{2}{w^2(t')}dt', \tag{A4}$$

$$\langle \theta_y y\rangle_{\rm av}=\int_0^t dt'\int_0^{t'}\frac{2}{w^2(t')}dt'=2\int_0^t\frac{t-t'}{w^2(t')}dt', \tag{A5}$$

$$\langle y^2\rangle_{\rm av}=\int_0^t dt'\int_0^{t'}dt'\int_0^{t'}\frac{4}{w^2(t')}dt'=2\int_0^t\frac{(t-t')^2}{w^2(t')}dt'. \tag{A6}$$

These formulas give other physical and mathematical meanings of Eyges' functions of $A_0(t)$, $A_1(t)$, and $A_2(t)$ [4]. Likewise

$$\frac{d}{dt}\langle \Delta_y\rangle_{\rm av}=\tfrac{1}{2}\langle \theta_y^2\rangle_{\rm av}, \tag{A7}$$

$$\langle \Delta_y\rangle_{\rm av}=\int_0^t dt'\int_0^{t'}\frac{1}{w^2(t')}dt'=\int_0^t\frac{t-t'}{w^2(t')}dt'. \tag{A8}$$

In the case of our approximation (2) of $w=2E/E_s$, we get

$$\langle \theta_y^2\rangle_{\rm av}=\frac{E_s^2}{2E_0\varepsilon}\left(\frac{E_0}{E}-1\right), \tag{A9}$$

$$\langle \Delta_y\rangle_{\rm av}=\tfrac{1}{2}\langle \theta_y y\rangle_{\rm av}=\frac{E_s^2}{4\varepsilon^2}\left(\frac{E}{E_0}-1+\ln\frac{E_0}{E}\right), \tag{A10}$$

$$\langle y^2\rangle_{\rm av}=\frac{E_s^2E_0}{2\varepsilon^3}\left\{1-\left(\frac{E}{E_0}\right)^2-\frac{2E}{E_0}\ln\frac{E_0}{E}\right\}. \tag{A11}$$

## APPENDIX B: MORE ACCURATE DERIVATION OF MEAN THICKNESSES AND EXCESSES OF THE PATH LENGTH THAN THE SMALL ANGLE APPROXIMATION

We make a more accurate evaluation of averaged thickness and the excess of the path length than the small angle approximation. We assume ionization loss to be proportional to the actual path length $s$:

$$dE=-\varepsilon ds. \tag{B1}$$

Under the Fokker-Planck approximation and our approximation (2) of $w=2E/E_s$,

$$d\langle \theta^2\rangle_{\rm av}=\frac{E_s^2}{E^2}ds, \tag{B2}$$

then

$$\frac{E}{E_0}=1-\frac{s}{R}, \tag{B3}$$

$$\langle \theta^2\rangle_{\rm av}=\frac{E_s^2}{E_0\varepsilon}\frac{s}{R}\Big/\left(1-\frac{s}{R}\right). \tag{B4}$$

The mean thickness $\langle t\rangle_{\rm av}$ and the mean excess $\langle \Delta\rangle_{\rm av}$ of the path length can be derived from

$$d\langle t\rangle_{\rm av}=\langle\cos\,\theta\rangle_{\rm av}ds, \tag{B5}$$

$$d\langle \Delta\rangle_{\rm av}=(1-\langle\cos\,\theta\rangle_{\rm av})ds. \tag{B6}$$

If we neglect the fluctuation of $\theta^2$, $\langle\cos\,\theta\rangle_{\rm av}$ can be approximated by

$$\langle\cos\,\theta\rangle_{\rm av}\cong\cos\langle\theta^2\rangle_{\rm av}^{1/2}. \tag{B7}$$

Then $\langle t\rangle_{\rm av}$ and $\langle \Delta\rangle_{\rm av}$ can be obtained numerically as

$$\langle t\rangle_{\rm av}=\int_0^s\cos\langle\theta^2\rangle_{\rm av}^{1/2}\,ds, \tag{B8}$$

$$\langle \Delta\rangle_{\rm av}=s-\langle t\rangle_{\rm av}. \tag{B9}$$

In the case where

$$E_0 \gg E_s^2/\varepsilon \quad \text{or} \quad s/R \ll 1, \tag{B10}$$

$\langle \theta^2 \rangle_{\rm av}$ is small enough, so we can approximate

$$\cos\langle \theta^2 \rangle_{\rm av}^{1/2} \cong 1 - \tfrac{1}{2}\langle \theta^2 \rangle_{\rm av}. \tag{B11}$$

Thus we get

$$\langle \Delta \rangle_{\rm av}/R = -\frac{E_s^2}{2E_0\varepsilon}\left[\frac{s}{R} + \ln\left(1 - \frac{s}{R}\right)\right], \tag{B12}$$

which is equivalent to the result (A10) indicated above and $\langle \Delta_{\rm I} \rangle_{\rm av}$ indicated in Table III if we read $s/R$ as the fraction of dissipated energy.

Another approximation instead of Eq. (B11),

$$\cos\langle \theta^2 \rangle_{\rm av}^{1/2} \cong [1 + \tfrac{1}{2}\langle \theta^2 \rangle_{\rm av}]^{-1} \tag{B13}$$

under the small angle approximation, gives an approximated formula,

$$\begin{aligned}\langle \Delta \rangle_{\rm av}/R = &\left(\frac{E_s^2}{2E_0\varepsilon} - 1\right)^{-1} \frac{E_s^2}{2E_0\varepsilon} \\ &\times \left\{ \frac{s}{R} - \left(\frac{E_s^2}{2E_0\varepsilon} - 1\right)^{-1} \right. \\ &\left. \times \ln\left[1 + \left(\frac{E_s^2}{2E_0\varepsilon} - 1\right)\frac{s}{R}\right]\right\},\end{aligned} \tag{B14}$$

which does not diverge at the limit as $s \to R$. But the accuracy of the result is not improved by the new approximation.

## APPENDIX C: INVERSE LAPLACE TRANSFORMS OF THE RELEVANT IMAGE FUNCTIONS

From the basic formula of inverse Laplace transforms [35]

$$\mathcal{L}^{-1}[(\sqrt{s} - a)^{-1} s^{-1/2} e^{-k\sqrt{s}}] = e^{a^2 t - ak}\ \mathrm{erfc}\left(\frac{k}{2\sqrt{t}} - a\sqrt{t}\right), \tag{C1}$$

we get the following formulas by sequential differentiations with $k$:

$$\begin{aligned}&\mathcal{L}^{-1}[(\sqrt{s} - a)^{-1} s^{1/2} e^{-k\sqrt{s}}] \\ &= a^2 e^{a^2 t - ak}\ \mathrm{erfc}\left(\frac{k}{2\sqrt{t}} - a\sqrt{t}\right) \\ &\quad + \frac{a}{\sqrt{\pi t}}\left(1 + \frac{k}{2at}\right) e^{-k^2/(4t)},\end{aligned} \tag{C2}$$

$$\begin{aligned}&\mathcal{L}^{-1}[(\sqrt{s} - a)^{-1} s e^{-k\sqrt{s}}] \\ &= a^3 e^{a^2 t - ak}\ \mathrm{erfc}\left(\frac{k}{2\sqrt{t}} - a\sqrt{t}\right) \\ &\quad + \frac{a^2}{\sqrt{\pi t}}\left(1 + \frac{ak - 1}{2a^2 t} + \frac{k^2}{4a^2 t^2}\right) e^{-k^2/(4t)},\end{aligned} \tag{C3}$$

$$\begin{aligned}&\mathcal{L}^{-1}[(\sqrt{s} - a)^{-1} s^{3/2} e^{-k\sqrt{s}}] \\ &= a^4 e^{a^2 t - ak}\ \mathrm{erfc}\left(\frac{k}{2\sqrt{t}} - a\sqrt{t}\right) + \frac{a^3}{\sqrt{\pi t}} \\ &\quad \times \left(1 + \frac{ak - 1}{2a^2 t} + \frac{ak - 3}{4a^3 t^2}k + \frac{k^3}{8a^3 t^3}\right) e^{-k^2/(4t)}.\end{aligned} \tag{C4}$$

Differentiating these formulas with $a$, we get

$$\begin{aligned}&\mathcal{L}^{-1}[(\sqrt{s} - a)^{-2} s^{1/2} e^{-k\sqrt{s}}] \\ &= a^2\left(2at - k + \frac{2}{a}\right) e^{a^2 t - ak}\ \mathrm{erfc}\left(\frac{k}{2\sqrt{t}} - a\sqrt{t}\right) \\ &\quad + \frac{2a^2}{\sqrt{\pi/t}}\left(1 + \frac{1}{2a^2 t}\right) e^{-k^2/(4t)},\end{aligned} \tag{C5}$$

$$\begin{aligned}&\mathcal{L}^{-1}[(\sqrt{s} - a)^{-2} s e^{-k\sqrt{s}}] \\ &= a^3\left(2at - k + \frac{3}{a}\right) e^{a^2 t - ak}\ \mathrm{erfc}\left(\frac{k}{2\sqrt{t}} - a\sqrt{t}\right) \\ &\quad + \frac{2a^3}{\sqrt{\pi/t}}\left(1 + \frac{1}{a^2 t} + \frac{k}{4a^3 t^2}\right) e^{-k^2/(4t)},\end{aligned} \tag{C6}$$

$$\begin{aligned}&\mathcal{L}^{-1}[(\sqrt{s} - a)^{-2} s^{3/2} e^{-k\sqrt{s}}] \\ &= a^4\left(2at - k + \frac{4}{a}\right) e^{a^2 t - ak}\ \mathrm{erfc}\left(\frac{k}{2\sqrt{t}} - a\sqrt{t}\right) \\ &\quad + \frac{2a^4}{\sqrt{\pi/t}}\left(1 + \frac{3}{2a^2 t} + \frac{2ak - 1}{4a^4 t^2} + \frac{k^2}{8a^4 t^3}\right) e^{-k^2/(4t)},\end{aligned} \tag{C7}$$

$$\begin{aligned}&\mathcal{L}^{-1}[(\sqrt{s} - a)^{-2} s^2 e^{-k\sqrt{s}}] \\ &= a^5\left(2at - k + \frac{5}{a}\right) e^{a^2 t - ak}\ \mathrm{erfc}\left(\frac{k}{2\sqrt{t}} - a\sqrt{t}\right) \\ &\quad + \frac{2a^5}{\sqrt{\pi/t}}\left(1 + \frac{2}{a^2 t} + \frac{3ak - 2}{4a^4 t^2}\right. \\ &\quad \left. + \frac{2ak^2 - 3k}{8a^5 t^3} + \frac{k^3}{16a^5 t^4}\right) e^{-k^2/(4t)}.\end{aligned} \tag{C8}$$

[1] B. Rossi and K. Greisen, Rev. Mod. Phys. **27**, 240 (1941).
[2] E. J. Williams, Proc. R. Soc. London **A169**, 531 (1939).
[3] W. T. Scott, Rev. Mod. Phys. **35**, 231 (1963).
[4] L. Eyges, Phys. Rev. **74**, 1534 (1948).
[5] C. N. Yang, Phys. Rev. **84**, 599 (1951).
[6] T. Nakatsuka, Phys. Rev. D **35**, 210 (1987).
[7] G. Molière, Z. Naturforsch. A **3A**, 78 (1948).
[8] H. A. Bethe, Phys. Rev. **89**, 1256 (1953).
[9] Particle Data Group, R. M. Barnett *et al.*, Phys. Rev. D **54**, 1 (1996), p. 132.
[10] G. Molière, Z. Naturforsch. A **10A**, 177 (1955).
[11] K. Kamata and J. Nishimura, Prog. Theor. Phys. Suppl. **6**, 93 (1958).
[12] J. Nishimura, in *Handbuch der Physik, Band 46*, edited by S. Flügge (Springer, Berlin, 1967), Tei 2, p. 1.
[13] W. T. Scott, Phys. Rev. **75**, 1763 (1949).
[14] L. Landau, J. Phys. (Moscow) **8**, 201 (1944).
[15] K. R. Symon, introduced by Rossi in Ref. [18].
[16] P. V. Vavilov, Zh. Eksp. Teor. Fiz. **32**, 920 (1957) [Sov. Phys. JETP **5**, 749 (1957)].
[17] K. A. Ispirian, A. T. Margarian, and A. M. Zverev, Nucl. Instrum. Methods **117**, 125 (1974).
[18] B. Rossi, *High Energy Particles* (Prentice-Hall, Englewood Cliffs, NJ, 1952).
[19] H. Bichsel and E. A. Uehling, Phys. Rev. **119**, 1670 (1960).
[20] M. J. Berger, in *Methods in Computational Physics*, edited by B. Adler, S. Fernbach, and M. Rotenberg (Academic, New York, 1962), Vol. I.
[21] H. A. Bethe and J. Ashkin, in *Experimental Nuclear Physics*, edited by E. Segre (Wiley, New York, 1959), Vol. 1, Part 2, p. 166.
[22] R. D. Birkhoff, in *Handbuch der Physik, Band 34*, edited by S. Flügge (Springer, Berlin, 1958), p. 53.
[23] S. M. Selzer and M. J. Berger, Nucl. Instrum. Methods **119**, 157 (1974).
[24] W. R. Nelson, H. Hirayama, and D. W. O. Rogers, ''The EGS4 Code System,'' SLAC-265, Stanford Linear Accelerator Center, 1985.
[25] S. M. Selzer, in *Monte Carlo Transport of Electrons and Photons Below 50 MeV*, edited by W. R. Nelson, T. M. Jenkins, A. Rindi, A. E. Nahum, and D. W. O. Rogers (Plenum, New York, 1989), pp. 153–182.
[26] J. A. Halbleib, R. P. Kensek, T. A. Mehlhorn, G. D. Valdez, S. M. Selzer, and M. J. Berger, ITS Version 3.0: The Integrated TIGER Series of Coupled Electron/Photon Monte Carlo Transport Codes, Sandia report SAND91-1634, 1992.
[27] M. Messel and D. F. Crawford, *Electron-Photon Shower Distribution Function Tables for Lead Copper and Air Absorbers* (Pergamon, Oxford, 1970).
[28] A. F. Bielajew and D. W. O. Rogers, Nucl. Instrum. Methods Phys. Res. B **18**, 165 (1987).
[29] T. Nakatsuka, in ''Nineteenth International Cosmic Ray Conference, La Jolla, California, 1985,'' Contribution No. HE 4.7-11 (unpublished); Uchusen-Kenkyu (printed from Institute for Cosmic Ray Research, University of Tokyo) **29**, 167 (1986).
[30] L. Landau, J. Phys. (Moscow) **3**, 237 (1940): Zh. Eksp. Teor. Fiz. **10**, 1007 (1940).
[31] Eyges proposed a similar approximation, regarding $\varepsilon$ as the constant rate of momentum loss and $w(t)=2(pc-\varepsilon t)/E_s$ in Ref. [4].
[32] $\tau$ is a half of the variable $y$, used in cascade shower theories, e.g., Ref. [1] and Ref. [12].
[33] The first and the second derivatives of $D$'s and $\Xi$'s, appearing later, are tabulated by T. Nakatsuka, in *25th International Cosmic Ray Conference*, Durban, South Africa, 1997, *Conference Papers*, edited by M. S. Potgieter, B. C. Raubenheimer, and D. J. van der Walt (Potchefstroomse Universiteit, Durban, 1997), Vol. 6, p. 301; or in T. Nakatsuka, *The First International Workshop on EGS4, KEK*, Tsukuba, 1997, KEK Proceedings 97-16, edited by H. Hirayama, Y. Namito, and S. Ban, High Energy Accelerator Research Organization, 1997, p. 109.
[34] The same probability density expressed in $u'$ can be compared in Fig. 1 of T. Nakatsuka, in *5th Asia Pacific Physics Conference, Kuala Lumpur, 1992, Conference Papers*, edited by S. P. Chia, K. S. Low, M. Othman, C. S. Wong, A. C. Chew, and S. P. Moo (World Scientific, Singapore, 1992), Vol. 1, p. 539.
[35] *Handbook of Mathematical Functions with Formulas, Graphs, and Mathematical Tables*, edited by M. Abramowitz and I. A. Stegun (Dover, New York, 1965), Chap. 29.